Organotransition-Metal Metallacarboranes. 37.[1] Paramagnetic Iron−Cobalt and Dicobalt Triple-Decker Sandwich Complexes

Martin Stephan,[2a,b] Peter Müller,[2a,b] Ulrich Zenneck,[2c] Hans Pritzkow,[2b] Walter Siebert,*[,2b] and Russell N. Grimes*[,2a]

Department of Chemistry, University of Virginia, Charlottesville, Virginia 22901, Anorganisch-Chemisches Institut der Universität, D-69120 Heidelberg, Germany, and Institut für Anorganische Chemie der Universität Erlangen-Nürnberg, D-91058 Erlangen, Germany

Received October 27, 1994[⊗]

A series of 2,3-C_2B_3-bridged iron−cobalt and dicobalt triple-decker complexes having Cp or Cp* end rings was examined in detail via several techniques, including correlated ^1H and ^{13}C NMR spectra, which allow complete assignment of the resonances of paramagnetic species. The 29 valence electron (ve) complexes Cp*Fe($Et_2C_2B_3H_2$-5-R)CoCp* (**1a**, R = H; **1b**, R = Cl; **1c**, R = Br) were prepared from *nido*-Cp*Co($Et_2C_2B_3H_4$-5-R) by bridge-deprotonation and treatment with $(Cp^*FeCl)_2$ and examined by cyclic voltammetry, ESR, and Mössbauer spectra and NMR correlation experiments. In the latter studies, paramagnetic neutral species were progressively reduced to the diamagnetic monoanions **1a**$^-$−**1c**$^-$ via repeated contact with a potassium mirror in the NMR tube or oxidized to the diamagnetic cations by treatment with $AgBF_4$. The data consistently support a model in which the unpaired electron in the neutral species **1a** is primarily associated with Fe; in the paramagnetic 31 ve dianion **1a**$^{2-}$, the unpaired electron resides mainly on cobalt. Correlated ^1H and ^{13}C NMR studies on the mixed-ligand 29 ve FeCo complex Cp*Fe($Et_2C_2B_3H_3$)CoCp (**2**) and the diamagnetic 30 ve dicobalt complexes Cp*Co($R'_2C_2B_3H_3$)CoCp* (**3a**, R′ = Et; **3b**, R′ = Me; **3c**, R′ = H) and Cp*Co($Et_2C_2B_3H_3$)CoCp (**4**), together with their associated cationic and anionic species, afforded additional information on the electronic structures of these systems. The preparation and spectroscopic characterization of the new complexes **1a**−**1c**, **2**, **3a**, and **3a**$^-$ are reported, as well as X-ray crystal structure determinations on a K(THF)(crown ether)$^+$ salt of **3a**$^-$ and neutral **4**. Crystal data for [K(THF)(crown ether)$^+$][**3a**$^-$]: $Co_2KO_7C_{42}B_3H_{75}$, space group $P2_12_12_1$ (orthorhombic); a = 15.252(14), b = 15.54(2), c = 20.25(2) Å; Z = 4; R = 0.046 for 6641 independent reflections. Crystal data for **4**: $Co_2C_{21}B_3H_{33}$, space group $P2_1/c$ (monoclinic); a = 8.694(4), b = 21.049(11), c = 11.870(8) Å; β = 101.15(4) Å; Z = 4; R = 0.039 for 4653 independent reflections.

Introduction

Multidecker sandwich complexes bridged by planar C_2B_3 (carborane),[3] C_4B (borole),[4] or C_3B_2 (diborole)[5] rings have been intensively studied both for their intrinsic theoretical interest and as possible building-blocks for polymers or solid-state materials having tailorable electronic and other properties.[6] The electronic structures and chemistry of these complexes are particularly conducive to detailed study: they are generally neutral, crystalline, air-stable, soluble in organic solvents and exhibit several reversibly accessible redox states. Even more importantly, known synthetic routes have made it possible to prepare *entire families* of multidecker sandwiches in which the metals and/or substituent groups are systematically varied.[6] This allows much more comprehensive and wide-ranging exploration of the nature of such complexes than would be possible on individual species.

Our groups have been involved in a cooperative effort to develop a more detailed picture of the electronic structure of 2,3-C_2B_3-bridged sandwich complexes. In this context, we have examined a series of paramagnetic FeCo and CoCo triple-decker metallacarboranes having a single unpaired electron.[7] Such compounds are of particular interest since they are amenable to study via NMR correlation and ESR techniques, affording insight into the shape of the MO occupied by the unpaired electron and the extent of the electron-delocalization between the metal centers.

Results and Discussion

Synthesis of Iron−Cobalt Triple-Decker Complexes. Although a C_2B_3-bridged iron−cobalt triple-decker, CpFe-

⊗ Abstract published in *Advance ACS Abstracts,* March 15, 1995.

(1) (a) Part 36: Houseknecht, K. L.; Stockman, K. E.; Sabat, M.; Finn, M. G.; Grimes, R. N. *J. Am. Chem. Soc.* **1995**, *117*, 1163. (b) Part 35: Stephan, M.; Hauss, J.; Zenneck, U.; Siebert, W.; Grimes, R. N. *Inorg. Chem.* **1994**, *33*, 4211. (c) Based in part on the Ph.D. dissertations of M.S. and P.M., Universität Heidelberg, 1992 and 1994, respectively.

(2) (a) University of Virginia. (b) Universität Heidelberg. (c) Universität Erlangen-Nürnberg.

(3) (a) Grimes, R. N. In *Electron-Deficient Boron and Carbon Clusters*; Olah, G. A., Wade, K., Williams, R. E., Eds.; John Wiley and Sons: New York, 1991; Chapter 11, pp 261−285. (b) Piepgrass, K. W.; Meng, X.; Hölscher, M.; Sabat, M.; Grimes, R. N. *Inorg. Chem.* **1992**, *31*, 5202. (c) Meng, X.; Sabat, M.; Grimes, R. N. *J. Am. Chem. Soc.* **1993**, *115*, 6143. (d) Wang, X.; Sabat, M.; Grimes, R. N. *J. Am. Chem. Soc.* **1994**, *116*, 2687.

(4) (a) Herberich, G. E.; Carstensen, T.; Koeffer, D. P. J.; Klaff, N.; Boese, R.; Hyla-Krypsin, I.; Gleiter, R.; Stephan, M.; Meth, H.; Zenneck, U. *Organometallics* **1994**, *13*, 619 and references therein. (b) Hyla-Krypsin, I.; Gleiter, R.; Herberich, G. E.; Benard, M. *Organometallics* **1994**, *13*, 1795. (c) Herberich, G. E. In *Comprehensive Organometallic Chemistry*; Wilkinson, G., Stone, F. G. A., Abel, E., Eds.; Pergamon Press: Oxford, England, 1982; Chapter 5.3.

(5) (a) Siebert, W. *Adv. Organomet. Chem.* **1993**, *35*, 187. (b) Siebert, W.; Herter, W.; Schulz, H.; Huck, S.; Pritzkow, H.; Zhu, L.; Eisenstein, O. *Chem. Ber.* **1993**, *126*, 1587 and references therein. (c) Siebert, W. *Angew. Chem., Int. Ed. Engl.* **1985**, *24*, 943 and *Pure Appl. Chem.* **1987**, *59*, 947.

(6) (a) Grimes, R. N. *Chem. Rev.* **1992**, *92*, 251. (b) Grimes, R. N. *Current Topics in the Chemistry of Boron*; Royal Society of Chemistry: Cambridge, England, 1994; p 269.

(7) (a) Presented in part at the Eighth International Meeting on Boron Chemistry (IMEBORON VIII), Knoxville, TN, July 1993; see *Abstracts of Papers*, No. CA-23. (b) Stephan, M.; Müller, P.; Zenneck, U.; Grimes, R. N.; Siebert, W. In *Current Topics in the Chemistry of Boron*; Kabalka, G. W., Ed.; Royal Society of Chemistry: Cambridge, England, 1994; p 326.

0020-1669/95/1334-2058$09.00/0

Scheme 1

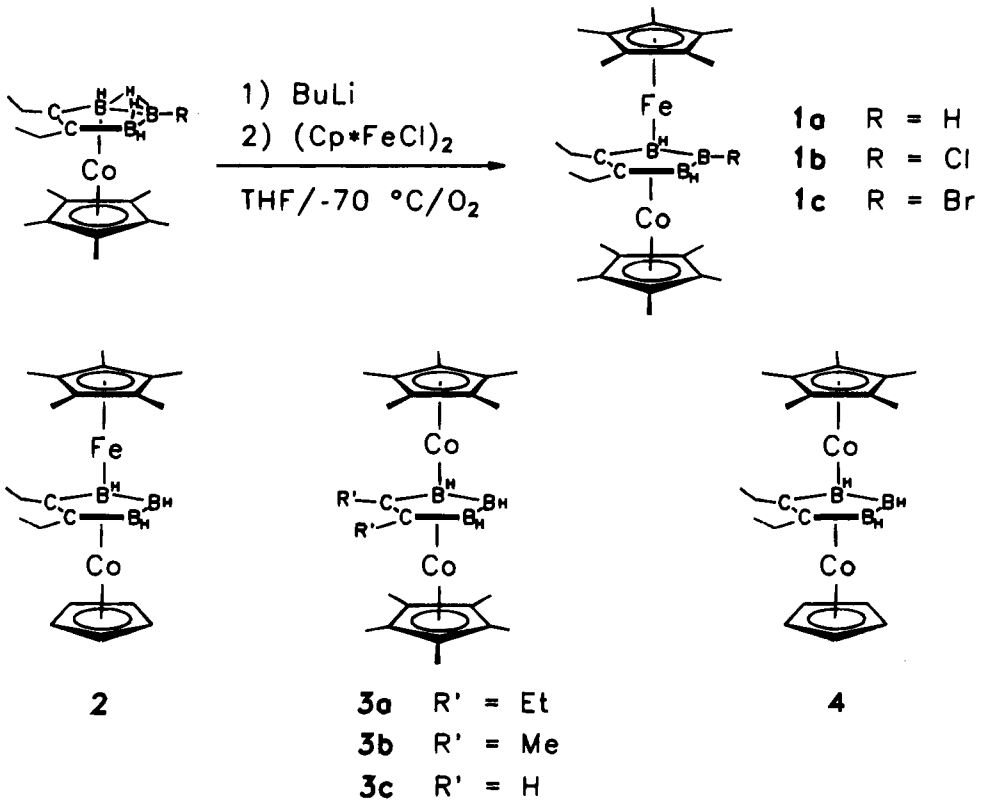

$(Et_2C_2B_3H_3)CoCp$, had earlier been synthesized in low yield via displacement of cyclooctatriene from the $[(\eta^6\text{-}C_8H_{10})Fe(Et_2C_2B_3H_4)]^-$ anion,[8] for the present study we adopted a different approach to prepare the analogous Cp* species (Cp* = η^5-C_5Me_5). The heterodinuclear triple-decker complexes $Cp^*Fe(Et_2C_2B_3H_2\text{-}5\text{-}R)CoCp^*$ (**1a**, R = H; **1b**, R = Cl; **1c**, R = Br) were generated from the corresponding precursor complexes *nido*-$Cp^*Co(Et_2C_2B_3H_4\text{-}5\text{-}R)$ by bridge-deprotonation and treatment with $(Cp^*FeCl)_2$ at −70 °C in THF followed by workup in air (Scheme 1). The new compounds were isolated via chromatography on silica and obtained in 62−93% yields as dark brown crystalline solids that survive exposure to air for months. An analogous species, dark brown, air-stable $Cp^*Fe(Et_2C_2B_3H_3)CoCp$ (**2**), was similarly prepared in 43% yield from the known complex[8] *nido*-$CpCo(Et_2C_2B_3H_5)$. For all compounds, the compositions were established from mass spectra and elemental analyses.

Redox Behavior. The properties of the 29-electron neutral complexes are clearly substituent-dependent. Compound **1a** was easily oxidized by 1 equiv of $AgBF_4$ in ether, forming the purple 28-electron monocation $\mathbf{1a}^+$ quantitatively; the same treatment of **1b** and **1c** gave ambiguous results. Cyclic voltammetry on **1a**, **1b**, and **1c** in dimethoxyethane (DME) showed reversible oxidation to the monocations and reduction to the diamagnetic 30-electron monoanions $\mathbf{1a}^-$ and $\mathbf{1b}^-$). In the case of **1a**, an irreversible second oxidation was observed and there was evidence of a reduction ($E_p^{red} < -3.1$ V) to the paramagnetic 31-electron dianion. For **1c**, the bromo substituent clearly affects the redox behavior: the reduction appears to be reversible, but the reduction wave is higher than the oxidation wave, suggesting that a second, irreversible reduction may be occurring at a potential only ca. 0.1 V more negative than the first. Table 1 presents the electrochemical data, and the CV plot for **1a** is shown in Figure 1. Not surprisingly, the presence of electron-withdrawing chloro and bromo substituents in **1b** and **1c** shifts their reduction potentials in a positive direction relative to that of **1a**. Also as expected, the 29-electron unsubstituted complex **1a** is more easily reduced (and more difficult to oxidize) than its 30-electron dicobalt counterpart $Cp^*Co(Et_2C_2B_3H_3)CoCp^*$ (**3a**), whose CV data are included in Table 1. However, the difference is not large (+0.30 vs +0.35 V) for the first oxidations of the neutral species), suggesting that the unpaired electron in **1a** is in a nonbonding orbital of relatively high energy.

Electron Spin Resonance Spectra. ESR data on complexes **1a**−**c** were obtained in toluene glass at 110−300 K (Table 2 and Figure 2). For comparison, the data for **2** are included, showing small differences produced by replacement of Cp with Cp*. No ^{59}Co hyperfine structure was observed, indicating that the unpaired electron is associated with the iron and not the cobalt atom, supporting a formal oxidation state of Fe(III). The axially symmetric spectra are closely comparable to those of several isoelectronic triple-decker sandwiches including the diborolyl−carboranyl "hybrid" species[9] $CpCo(Et_2MeC_3B_2Et_2)Fe(Et_2C_2B_4H_4)$ and the diiron diborolyl compound[10] $CpFe(Et_2MeC_3B_2Et_2)FeCp$, taken under identical conditions, as well as the double-decker complexes[11,12] $Cp^*Fe(Et_2C_2B_4H_4)$ and $[(\eta^6\text{-}C_6Me_6)Fe(Et_2C_2B_4H_4)]^+$. The remarkable resemblance in these spectra strongly suggests similar electronic structures among this group of Fe(III) sandwich complexes and underlines the isolobal relationship among the apical BH, CoCp, CoCp*, and Fe(arene) units, all of which are formal 2-electron donors.

(8) Davis, J. H., Jr.; Sinn, E.; Grimes, R. N. *J. Am. Chem. Soc.* **1989**, *111*, 4776.
(9) Attwood, M. D.; Fonda, K. K.; Grimes, R. N.; Brodt, G.; Hu, D.; Zenneck, U.; Siebert, W. *Organometallics* **1989**, *8*, 1300.
(10) Brodt, G. Ph.D. Dissertation, Universität Heidelberg, 1988.
(11) Stephan, M.; Davis, J. H., Jr.; Meng, X.; Chase, K. P.; Hauss, J.; Zenneck, U.; Pritzkow, H.; Siebert, W.; Grimes, R. N. *J. Am. Chem. Soc.* **1992**, *114*, 5214.
(12) Merkert, J. M.; Geiger, W. E.; Attwood, M. D.; Grimes, R. N. *Organometallics* **1991**, *10*, 3545.

Table 1. Electrochemical Data for Triple-Decker Complexes[a]

complex	solvent[b]	couple	E° [c]	ΔE_p [d]	current ratio[e]	ν[f]
Cp*Fe($Et_2C_2B_3H_3$)CoCp* (**1a**)	DME	2+/+	+1.36	*g*		0.1
	DME	+/0	+0.35	80	0.96	0.05−5
	DME	0/−	−1.51	80	0.96	0.05−5
	DCM	+/0	+0.16	65	0.96	0.05−1
	DCM	0/−	−1.48	65	0.97	0.05−1
Cp*Fe($Et_2C_2B_3H_2$-5-Cl)CoCp* (**1b**)	DME	+/0	+0.50	97	0.98	0.05−0.5
	DME	0/−	−1.34	100	0.97	0.05−0.5
Cp*Fe($Et_2C_2B_3H_2$-5-Br)CoCp* (**1c**)	DME	+/0	+0.55	96	0.99	0.05−0.5
	DME	0/−	−1.05	*h*		0.05−0.5
1a$^+$	DCM	2+/+	+1.59/ +1.44	*g*		0.2
	DCM	+/0	+0.19	64	0.95	0.05−0.5
	DCM	0/−	−1.53	70	0.95	0.05−0.5
1a$^+$	AN	2+/+	+1.26	*g*		0.1
	AN	+/0	+0.15	80	0.98	0.05−0.5
	AN	0/−	−1.51	72	0.92	0.05−0.5
	AN	−2/−	*i*			
Cp*Co($Et_2C_2B_3H_3$)CoCp* (**3a**)	DME	2+/+	+1.49	*g*		0.1
	DME	+/0	+0.30	79	0.98	0.1−2
	DME	0/−	−2.00	76	0.96	0.1−2
	DMF	2+/+	+1.39	*g*		0.1
	DMF	+/0	+0.25	64	0.97	0.1−1
	DMF	0/−	−1.88	64	0.95	0.1−1

[a] Data reported for platinum disk working electrodes at room temperature; electrolyte [Bu_4N][PF_6], 0.1 M. [b] DME = dimethoxyethane, DCM = dichloromethane, AN = acetonitrile, DMF = dimethylformamide. [c] Volts vs saturated calomel electrode (SCE); E° reported for reversible systems, peak potentials (E_p^{ox}, E_p^{red}) for irreversible systems. [d] Separation in mV of anodic and cathodic peaks. [e] Ratio is given as i_a/i_c for reductions, i_c/i_a for oxidations. [f] Scan rate in V s^{-1}. [g] Irreversible. [h] Partly reversible; see text. [i] No reduction observed to −3.0 V.

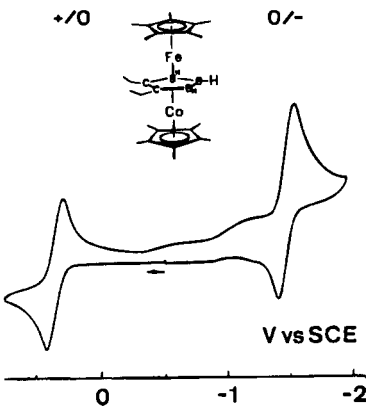

Figure 1. Cyclic voltammogram of Cp*Fe($Et_2C_2B_3H_3$)CoCp* (**1a**) in dimethoxyethane (DME, 298 K), recorded at Pt electrodes vs saturated calomel electrode (SCE) (ν = 0.1 V s^{-1}) in 0.1 M Bu_4NPF_6.

Table 2. ESR Data in Toluene Glass at 110 K

compd	$\langle g \rangle$	g_1 ($g_{\parallel}$)	g_2 ($g_{\perp}$)	g_3
1a	2.12	2.400	2.035	1.992
1b	2.16	2.455	2.031	
1c	2.16	2.500	2.030	
2	2.21	2.38	2.04	

Reduction of **1a** in THF solution by potassium initially gave the green, diamagnetic, ESR-inactive monoanion, which on further reduction produced red-brown **1a**$^{2-}$. The ESR spectrum of this 31 ve species exhibits ^{59}Co hyperfine splitting, indicating association of the unpaired electron with cobalt; however, the spectrum also reveals the presence of minor components that are taken to be cobalt-containing decomposition products. These species also give rise to signals that appear in the proton NMR spectra and increase over time, accompanied by decreasing intensity for the resonances of **1a**$^{2-}$.

Mössbauer Spectra. The ESR findings are augmented by Mössbauer data on **1a** (Figure 3) and **1b** which exhibit isomer shifts and quadrupole couplings in the range of previously studied 29-electron triple-decker and 17-electron double-decker Fe(III) sandwich systems.[13,14] Both spectra show doublets, but

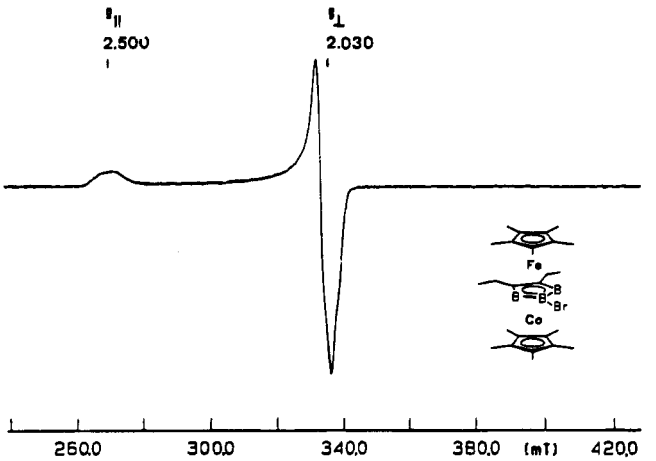

Figure 2. X-Band ESR spectrum of **1c** in toluene glass at 110 K referenced to LiTCNQ; $\langle g \rangle$ = 2.0025.

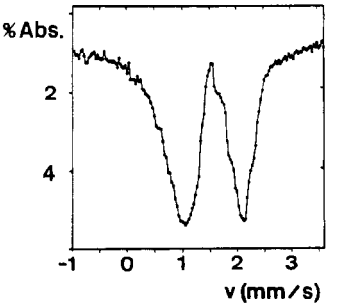

Figure 3. Mössbauer spectrum of **1a**.

the isomer shift and quadrupole splitting observed for **1a** (IS = 1.591 mm s^{-1}); ΔE^Q = 1.687 mm s^{-1}) are much larger than those of **1b**, whose corresponding values are 1.025 and 0.736 mm s^{-1}, respectively. This finding is in accord with the presence of an electron-withdrawing chloro substituent on **1b**.

^{1}H NMR Studies. Paramagnetic sandwich species typically exhibit essentially uninterpretable NMR spectra, but in recent work in our groups we have circumvented this problem via the

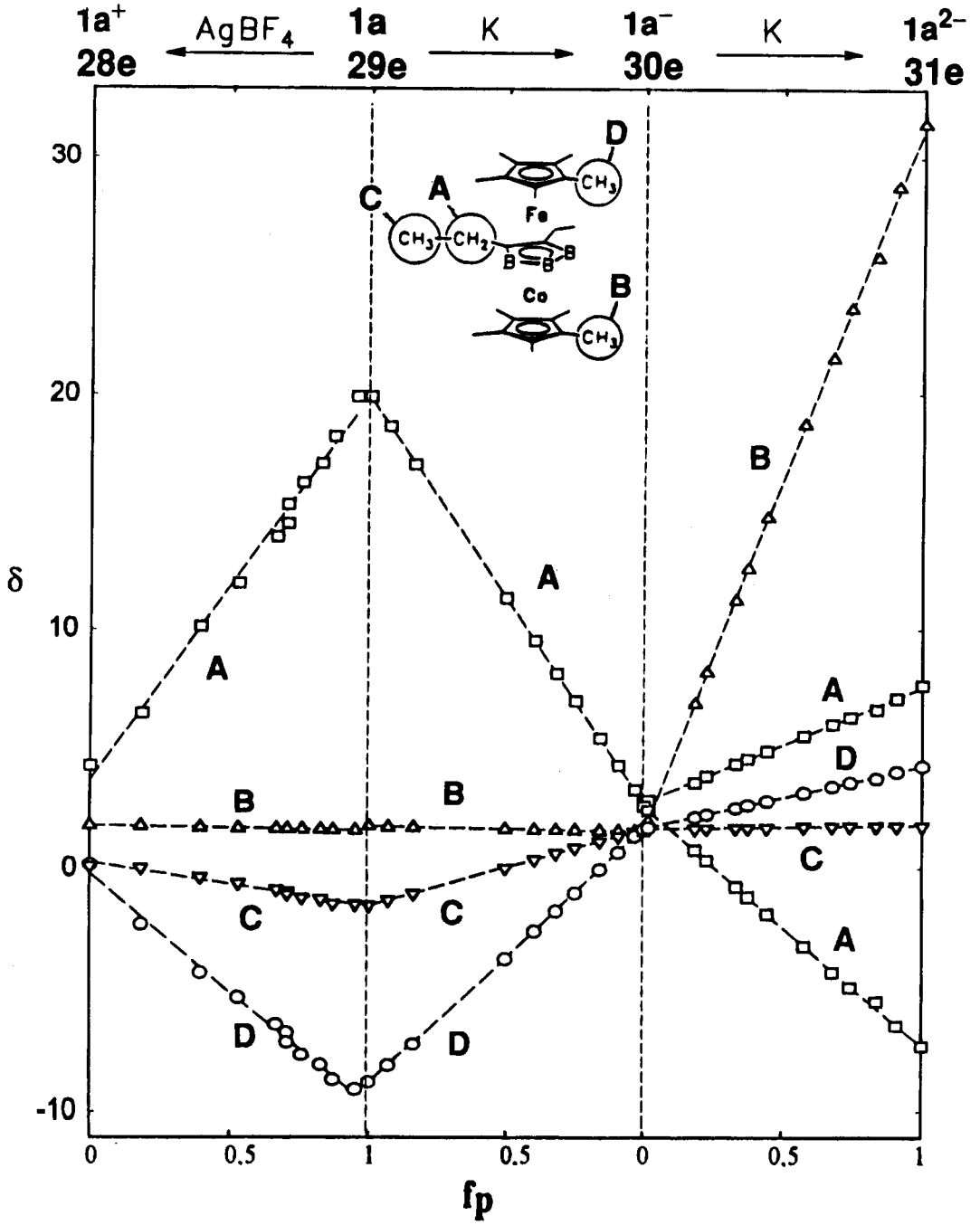

Figure 4. Correlation diagram for ^{1}H NMR spectra of **1a**$^+$/**1a**/**1a**$^-$/**1a**$^{2-}$ in $CDCl_3$ (for the oxidation of **1a**) and THF-d_8 (for the reductions). Value of δ (vertical axis) are plotted vs the mole fraction of the paramagnetic component (f_p).

technique of correlated spectroscopy, in which a paramagnetic complex is reduced *in situ* in stepwise fashion via repeated short exposure to a potassium mirror in a sealed tube, and the process monitored by ^{1}H and/or ^{13}C NMR.[1b,11,15] Signals from the paramagnetic species are thereby directly correlated with the corresponding peaks in the diamagnetic complex, allowing in most cases complete assignment of the paramagnetic spectrum and, in addition, providing information about the electronic structures of the species involved. In the present study the method was applied to the FeCo and corresponding CoCo triple-decker systems and for the first time (to our knowledge) has been used to correlate four different oxidation states in an organometallic system. Complete NMR data for all systems examined are tabulated as supplementary material.

Figure 4 shows the correlation diagram for the reduction of the 29-electron neutral complex **1a** to its 30-electron monoanion and 31-electron dianion, and the oxidation to the 28-electron cation. In the latter case, spectra were obtained for **1a**/**1a**$^+$ mixtures of known concentration ratios that were prepared via chemical oxidization of **1a** with $AgBF_4$. As shown, plots of proton NMR shifts (δ) on the vertical axis vs mole fraction of the paramagnetic component (f_p) are linear, each value of f_p generating an averaged set of signals indicating rapid electron transfer between the species present; thus one does not see the superimposed spectra of species corresponding to different

(13) Edwin, J.; Bochmann, M.; Boehm, M. C.; Brennan, D. E.; Geiger, W. E., Jr.; Krüger, C.; Pebler, J.; Pritzkow, H.; Siebert, W.; Swiridoff, W.; Wadepohl, H.; Weiss, J.; Zenneck, U. *J. Am. Chem. Soc.* **1983**, *105*, 2582.
(14) Wadepohl, H. Ph.D. Dissertation, Universität Marburg, Germany, 1982.
(15) (a) Koehler, F. H.; Zenneck, U.; Edwin, J.; Siebert, W. *J. Organomet. Chem.* **1981**, *208*, 137. (b) Zwecker, J.; Kuhlmann, T.; Pritzkow, H.; Siebert, W.; Zenneck, U. *Organometallics* **1988**, *7*, 2316.

oxidation states, as would be observed in the absence of rapid transfer. The individual proton resonances are easily identified from their shifts and integrated areas in the spectra of diamagnetic $\mathbf{1a}^-$ and $\mathbf{1a}^+$. The plots are informative with respect to the delocalization of the unpaired electron and the nature of the MO it occupies in the 29- and 31-electron paramagnetic species. In general, it can be assumed that the greater the interaction between the electron and a given proton, the larger will be the observed shift.[16] The carborane ethyl CH_3 protons are virtually unaffected by reduction or oxidation, but the CH_2 signals, in contrast, are highly sensitive since these protons are close to the center of the molecule where the spin density of the unpaired electron is localized. The two diastereotopic methylene proton signals in $\mathbf{1a}^{2-}$ are shifted in opposite directions, whereas both appear at the same frequency in neutral **1a**. The reason for this finding is not yet clear, but it underscores the high sensitivity of paramagnetic NMR shifts to changes in molecular electronic structure.

In neutral **1a** the unpaired electron is clearly much more closely associated with iron than cobalt, as the Cp*Co proton shifts are nearly unchanged by addition or removal of an electron while the Cp*Fe signal is sharply affected by both redox processes. In the 31-electron dianion the situation is reversed: here the Cp*Co protons show much higher sensitivity toward oxidation than do their Cp*Fe counterparts. These findings are consistent with the ESR spectra discussed above, which suggest that the unpaired electron in **1a** is in a HOMO located mainly on Fe while the LUMO is primarily associated with cobalt. Hence it is reasonable to formulate **1a** as $Cp^*Fe^{III}(Et_2C_2B_3H_2$-5-R)$Co^{III}Cp^*$ and $\mathbf{1a}^{2-}$ as $[Cp^*Fe^{II}(Et_2C_2B_3H_2$-5-R)$Co^{II}Cp^*]^{2-}$. This picture is supported by the observation of cobalt hyperfine splitting in the ESR spectrum of $\mathbf{1a}^{2-}$.

Further insight into the electronic structures of these systems can be gained from the mixed-ligand complex **2** and its dicobalt counterpart $Cp^*Co(Et_2C_2B_3H_3)CoCp$ (**4**), whose correlated NMR spectra reveal major differences in the behavior of Cp* vs Cp proton shifts. As shown in Figure 5 (top), the reduction of neutral **4** to the monoanion produces a strong upfield shift for the CpCo signal and a moderate downfield shift for the Cp*Co resonance; in the homoligand species **3a** (Figure 5, bottom), the Cp* proton signal is similarly deshielded on reduction. These findings are interpreted as reflecting greater electron donation by the Cp* ligand to its coordinated metal (relative to Cp) as a result of which reduction occurs mainly at the less electron-rich CpCo center. The $-CH_2-$ resonances were not observed in this case, probably as a consequence of the broadness of these signals, their relative weakness (few nuclei are involved), and the fact that the methylene protons are close to the paramagnetic center.

The splitting of the methylene proton signal of **4** during reduction (plots labeled D in Figure 5, top) can be explained in terms of an ABX_3 spin system. In neutral **4** the resonances of the diastereotopic CH_2 protons are effectively superimposed, but as reduction occurs, the spin density of the unpaired electron on the CpCo and Cp*Co metal centers is slightly different, creating nonidentical environments for the methylene hydrogens. (In the region between f_p 0.16 and 0.59, these signals were not clearly detectable and are omitted in Figure 5 and the accompanying table in the supplementary material.) The large upfield shift of the CH_2 proton signals is similar to that of the CH_3 protons in the *C,C'*-dimethyl complex **3b**, reflecting similar effects of spin density and orientation of the unpaired electron on these protons.

(16) Rettig, M. F.; Drago, R. S. *J. Am. Chem. Soc.* **1969**, *91*, 1361.

A qualitatively analogous result is seen on reduction of **2** to diamagnetic $\mathbf{2}^-$ (Figure 6), in which the Cp*Fe proton signal is strongly shifted to lower field while the CpCo resonance shows a slight change in the opposite direction. Further reduction to the dianion produces a small further deshielding of the Cp*Fe protons. The NMR data for **2** are consistent with those for **1a** and confirm the assignment of the signals for the two different MCp* moieties; hence the resonances of CoCp and FeCp* in **2** are easily distinguished. Curiously, the observation of two distinct CH_2 signals for $\mathbf{1a}^{2-}$ (Figure 4) is not seen for $\mathbf{2}^{2-}$.

The consequences of changing the substituent on the cage carbons in the dicobalt system were explored to a limited degree by comparing the correlated NMR data for the *C,C'*-diethyl complex **3a** (Figure 5, bottom) with those of the *C,C'*-dimethyl derivative **3b** and the *C,C'*-dihydrogen species **3c**, both presented in Figure 7. A priori, one expects to find larger deshielding of the Cp* protons on reduction of **3c**, which has no ring substituents, than of **3a** and **3b**, whose electron-donating alkyl groups would tend to mitigate the Cp*-to-cobalt electron transfer. Although the effect is not a large one, the nearly 80 ppm shift in **3c** is in fact slightly greater than those of **3a** and **3b** (ca. 70 ppm). As a consequence of line broadening, the CH proton signals in **3c** were not observed.

^{13}C NMR Studies. Correlated carbon NMR spectra of the $Cp^*_2Co_2(R_2C_2B_3H_3)$ complexes were obtained, affording additional information on electronic structure. For each of the three species **3a–c**, reduction of the neutral 30-electron complex to the 31-electron monoanion produced a very pronounced shift (ca. 250 ppm) to higher field for the Cp* methyl carbon nuclei (Figure 8). This observation further supports the hypothesis that the added electron occupies a molecular orbital that is centered primarily on cobalt having strong interaction with the Cp* ligands. Oxidation of the neutral complexes **3a** and **3b** to their respective 29-electron cations produced consistent though less dramatic effects in the ^{13}C spectra. In both cases, the Cp* methyl carbon signals exhibit slight upfield shifts while the Cp* ring carbon resonances move downfield, suggesting that oxidation occurs mainly at a nonbonding orbital on cobalt. As in the proton NMR correlations (Figure 5), not all of the expected ^{13}C signals could be clearly observed, owing to line broadening and/or other factors previously mentioned.

X-ray Crystallographic Studies. Although a number of crystal structures of carborane-bridged triple-decker sandwiches have been obtained,[8,17] none having Cp* ligands has been reported. In order to probe possible structural changes effected by redox processes in the dicobalt species, structure determinations were conducted on the neutral compounds **3a** and **4** and on a THF–crown ether potassium salt of the anionic dicobalt complex $\mathbf{3a}^-$, the first ionic carborane multidecker sandwich to be structurally characterized. Unfortunately, disorder problems in the salts of the dicobalt triple-decker cations and in **1a** and **1b** prevented definitive crystallographic studies on any of those species, although low-quality X-ray data on $\mathbf{3a}^+BF_4^-$ revealed no major structural differences from the neutral complex.

The cluster geometries of the two neutral dicobalt compounds are closely similar, as expected, given that they differ only by

(17) (a) Beer, D. C.; Miller, V. R.; Sneddon, L. G.; Grimes, R. N.; Mathew, M.; Palenik, G. J. *J. Am. Chem. Soc.* **1973**, *95*, 3046. (b) Robinson, W. T.; Grimes, R. N. *Inorg. Chem.* **1975**, *14*, 3056. (c) Pipal, J. R.; Grimes, R. N. *Inorg. Chem.* **1978**, *17*, 10. (d) Davis, J. H., Jr.; Sinn, E.; Grimes, R. N. *J. Am. Chem. Soc.* **1989**, *111*, 4784. (e) Chase, K. J.; Bryan, R. F.; Woode, M. K.; Grimes, R. N. *Organometallics* **1991**, *10*, 2631. (f) Stockman, K. E.; Sabat, M.; Finn, M. G.; Grimes, R. N. *J. Am. Chem. Soc.* **1992**, *114*, 8733. (g) Butcher, R. J.; Darby, W. L.; Sinn, E. *Inorg. Chim. Acta* **1993**, *203*, 51.

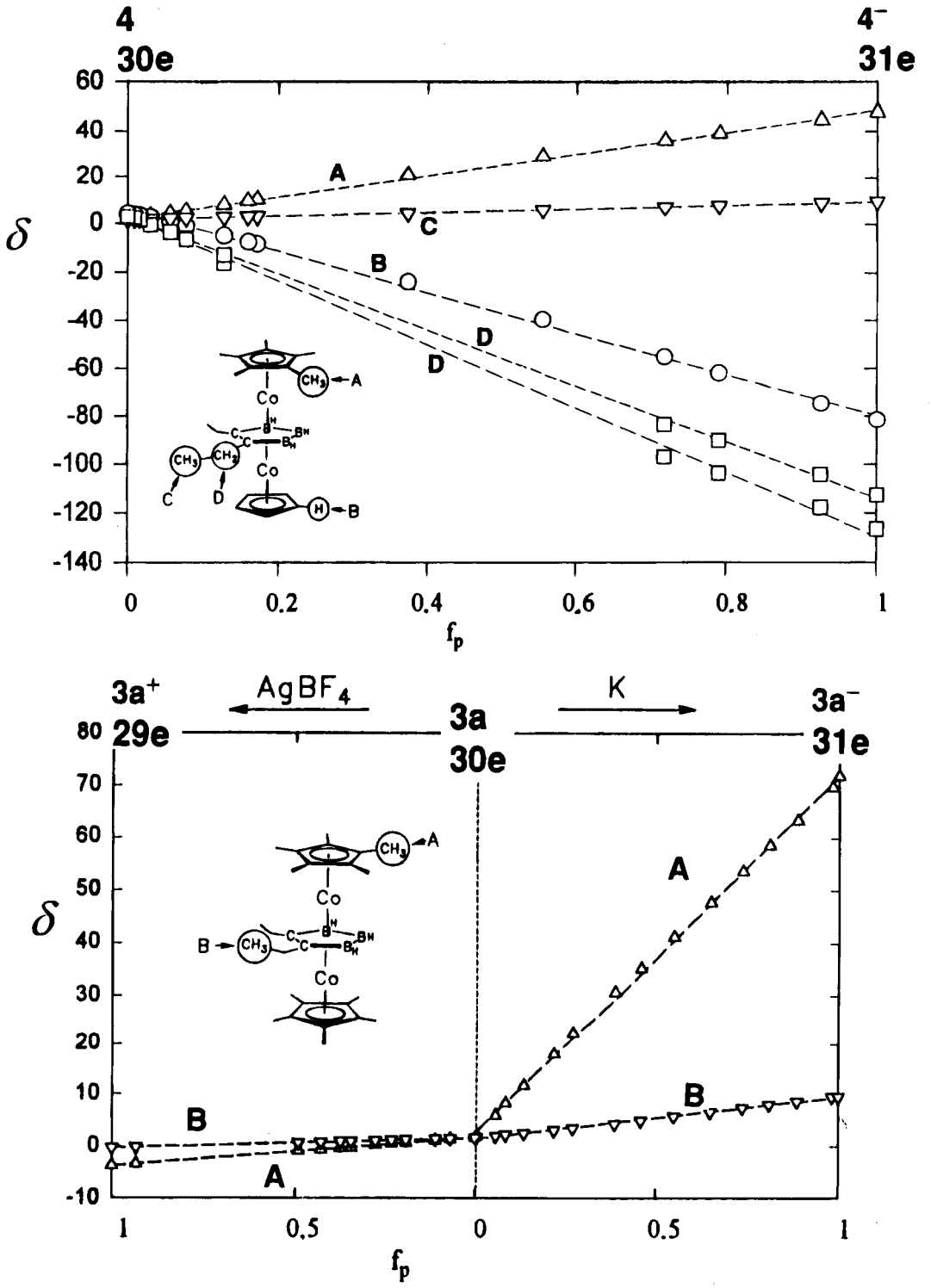

Figure 5. Correlation diagrams for ^{1}H NMR spectra of **4**/**4**$^-$ in THF-d_8 (top) and **3a**$^+$/**3a**/**3a**$^-$ in $CDCl_3$ for the oxidation and THF-d_8 for the reduction (bottom).

replacement of one Cp* by Cp. Since the data set obtained for **4** is superior to that of **3a**, we report the former structure in detail here (information on the **3a** structure has been deposited as supplementary material). ORTEP diagrams of the anion and the neutral complex are shown in Figures 9 and 10, respectively, while data collection and crystal information, atomic coordinates, bond distances, and bond angles are presented in Tables 3–5. Tables of positional and thermal parameters and mean planes, as well as an ORTEP diagram of the (THF)(crown ether)potassium cation, are provided as supplementary material. The structure of **4** closely resembles those of other neutral dicobalt C_2B_3-bridged triple-decker sandwiches,[8,17] with a Co–Co distance of 3.15 Å and comparable Co–B, Co–C, B–B, and B–C bond lengths. The Cp and Cp* ring planes are slightly tilted away from the carborane *C*-ethyl groups, with Cp*–C_2B_3 dihedral angles of 7.8 and 6.5°, and the C(2)–C(3) cage carbon distance is 1.471(4) Å, both within the normal range for this class. However, the molecular geometry of the $Co_2C_2B_3$ cluster in **3a**$^-$ differs slightly but significantly from that of **4**, revealing the effects of the additional negative charge (as previously noted, the replacement of one Cp* unit by Cp in **4** has negligible effect on the cobaltacarborane core structure). Thus, the cobalt atoms in **3a**$^-$ are significantly further from the C_2B_3 plane (⟨1.637(3) Å⟩) than are the cobalts in **4** (⟨1.577(3) Å⟩); the metal–Cp*

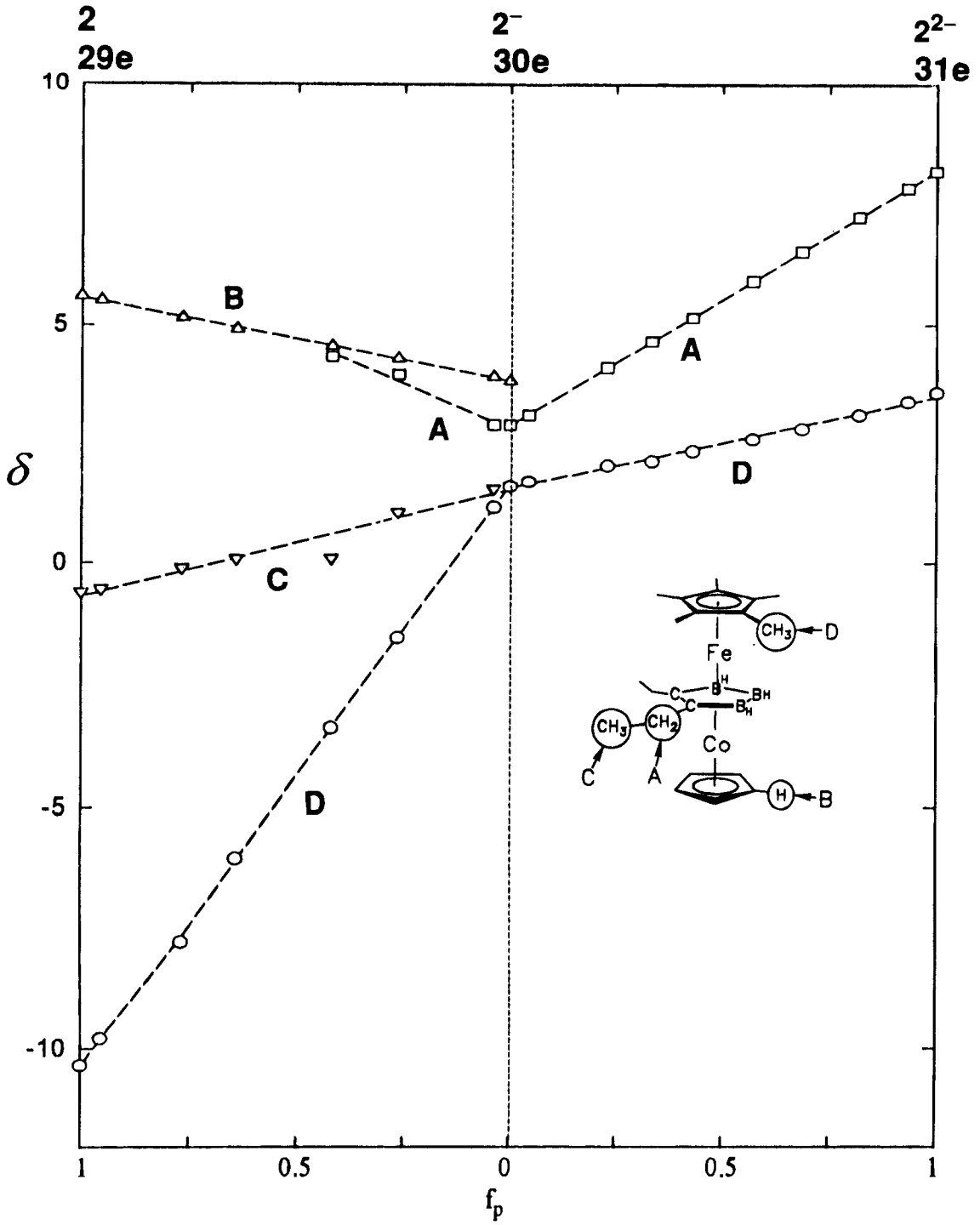

Figure 6. Correlation diagram for ^{1}H NMR spectra of **2**/**2**$^-$/**2**$^{2-}$ in THF-d_8.

(or Cp) distances are also slighlty greater in **3a**$^-$ than in **4** (⟨1.696(3)⟩ vs ⟨1.658(3) Å⟩). Also, the tilt of the Cp* planes in the anion with respect to the central ring is smaller (⟨5.5°⟩) than that in the neutral compound. These differences in the two structures are taken to reflect the structural consequences of reducing a 30-electron to a 31-electron system, with the added electron populating a C_2B_3−Co−Cp* antibonding orbital and thereby slightly lowering the average Co−ring atom bond order.

Experimental Section

The procedures and instrumentation employed in the syntheses and characterizations of new compounds are described in recent papers.[3b,c] The techniques utilized in the ESR, NMR, and electrochemical studies have been reported elsewhere.[11] The *nido*-Cp*Co($Et_2C_2B_3H_4$-5-R) complexes (R = H, Cl, Br) were prepared according to the literature method.[18] Compounds **3b**,[19] **3c**,[20] and **4**[21] were available from earlier studies. Except where otherwise indicated, all syntheses were conducted under vacuum or an atmosphere of nitrogen. Workup of products was generally conducted in air using benchtop procedures. Elemental analyses were obtained at the University of Virginia on a Perkin-Elmer 2400 CHN Analyzer using cyclohexanone 2,4-dinitrophenylhydrazone as a standard and (for **1a**−**c**) at the microanalysis laboratory of the

(18) (a) Davis, J. H., Jr.; Attwood, M. D.; Grimes, R. N. *Organometallics* **1990**, *9*, 1171. (b) Piepgrass, K. W.; Grimes, R. N. *Organometallics* **1992**, *11*, 2397. (c) Piepgrass, K. W.; Stockman, K. E.; Sabat, M.; Grimes, R. N. *Organometallics* **1992**, *11*, 2404.
(19) Finster, D. C.; Sinn, E.; Grimes, R. N. *J. Am. Chem. Soc.* **1981**, *103*, 1399.
(20) Benvenuto, M. A.; Sabat, M.; Grimes, R. N. *Inorg. Chem.* **1992**, *31*, 3904.
(21) Piepgrass, K. W.; Curtis, M. A.; Wang, X.; Meng, X.; Sabat, M.; Grimes, R. N. *Inorg. Chem.* **1993**, *32*, 2156.

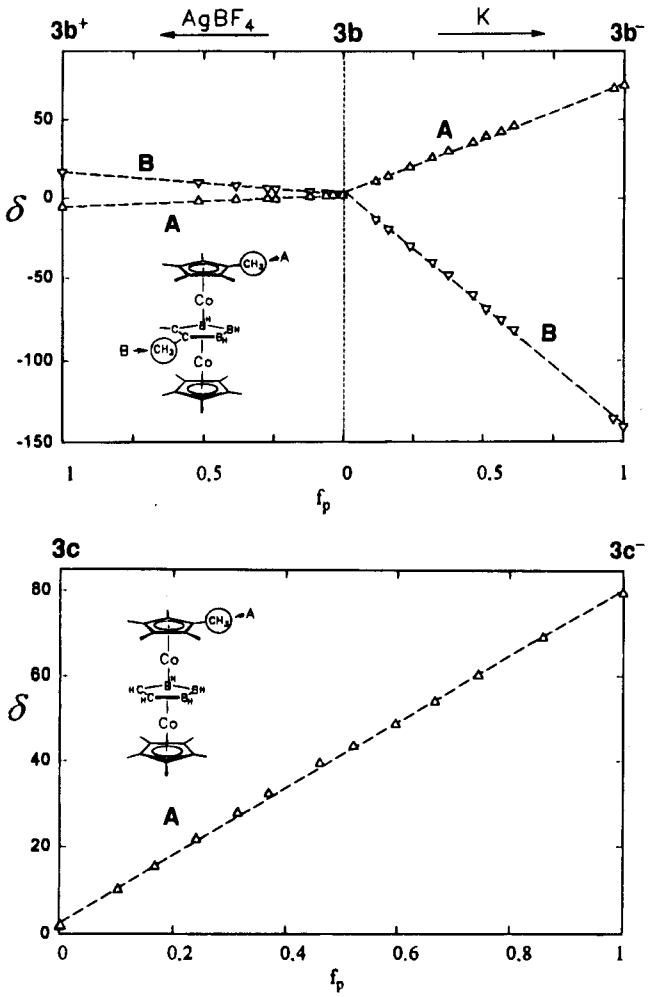

Figure 7. Correlation diagrams for ^{1}H NMR spectra of **3b**$^+$/**3b**/**3b**$^-$ in $CDCl_3$ for the oxidation and THF-d_8 for the reduction (top) and for **3c**/**3c**$^-$ in THF-d_8 (bottom).

Anorganisch−Chemisches Institut der Universität Heidelberg using a Heraeus CHN-O-Rapid instrument.

Synthesis of Cp*Fe($Et_2C_2B_3H_3$)CoCp* (1a). A solution of $(Cp^*FeCl)_2$ in THF was prepared via addition of 1 equiv of Cp*Li to a suspension of $FeCl_2$·(161 mg, 1.27 mmol) in THF at 0 °C followed by stirring for 1 h, after which the olive-green solution was frozen in liquid N_2. Separately, 400 mg (1.27 mmol) of Cp*Co($Et_2C_2B_3H_5$) was dissolved in 50 mL of THF and deprotonated with 1 equiv of *tert*-butyllithium. This solution was stirred for 1 h and added to the frozen solution of $(Cp^*FeCl)_2$, and the mixture was placed in a −78 °C bath and stirred overnight as it warmed to room temperature. The solvent was removed by rotary evaporation and the red-brown residue was taken up in CH_2Cl_2 and chromatographed on a 15 × 2.5 cm silica column. Elution with *n*-hexane afforded 100 mg (0.32 mmol) of recovered starting cobaltacarborane, and elution with CH_2Cl_2 gave a dark brown fraction consisting of **1a** (355 mg, 0.71 mmol, 74% yield based on starting material consumed). ^{1}H NMR (200 MHz) (δ, ppm): in $CDCl_3$, 18.32 (s, br), 1.56 (s, br, 15H), −1.47 (s, br, 6H); in THF-d_8, 19.90 (s, br, 4H, ethyl CH_2), 1.73 (s, br, 15H, Cp*Co), −1.50 (s, br, 6H, ethyl CH_3), −8.82 (s, br, 15H, Cp*Fe). IR (CH_2Cl_2, cm^{-1}): ν_{BH} = 2466 (m), 2360 (s), 2340 (s). Unit-resolution mass spectrum: parent envelope at *m/z* 503 (base peak). Exact mass: calcd for $^{59}Co^{56}Fe^{12}C_{26}{}^{11}B_3{}^1H_{43}{}^+$, 503.2325; found, 503.2315. Anal. Calcd for $CoFeC_{26}B_3H_{43}$: C, 62.10; H, 8.62. Found: C, 62.16; H, 8.88.

Synthesis of Cp*Fe($Et_2C_2B_3H_2$-5-Cl)CoCp* (1b). The same procedure employed for the preparation of **1a** using 150 mg (0.43 mmol) of Cp*Co($Et_2C_2B_3H_2$-5-Cl) gave 70 mg (0.2 mmol) of recovered starting material and 100 mg (0.19 mmol) of **1b** (93% based on starting cobaltacarborane consumed). ^{1}H NMR (200 MHz) (δ, ppm, in $CDCl_3$): 16.71 (s, br), 1.00 (s, br, 15H, Cp*), −2.08 (s, br, 6H, ethyl CH_3), −12.04 (s, br, 15H, Cp*). IR (CH_2Cl_2, cm^{-1}): ν_{BH} = 2479 (s), 2349 (s), 2283 (s). Unit-resolution mass spectrum: parent envelope at *m/z* 537 (base peak), no fragmentation. Exact mass: calcd for $^{59}Co^{56}Fe^{37}Cl^{12}C_{26}{}^{11}B_3{}^1H_{42}{}^+$, 539.1906; found, 539.1889.

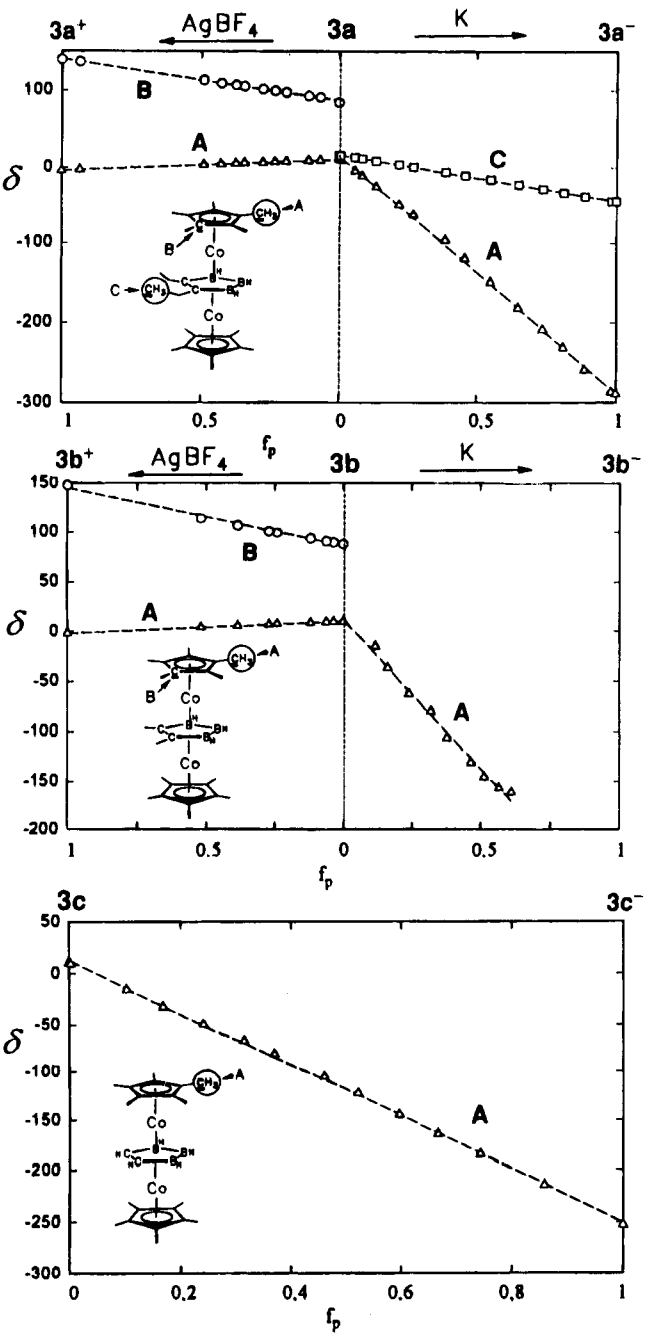

Figure 8. ^{13}C NMR correlation diagrams: top, **3a**$^+$/**3a**/**3a**$^-$ in $CDCl_3$ for the oxidation and THF-d_8 for the reduction; center, **3b**$^+$/**3b**/**3b**$^-$ in the same solvents; bottom, **3c**/**3c**$^-$ in THF-d_8.

Synthesis of Cp*Fe($Et_2C_2B_3H_2$-5-Br)CoCp* (1c). The same method employing 196 mg (0.50 mmol) of Cp*Co($Et_2C_2B_3H_2$-5-Br) gave 55 mg (0.14 mmol) of recovered starting material and 131 mg (0.22 mmol) of **1b** (62% based on starting cobaltacarborane consumed). ^{1}H NMR (200 MHz) (δ, ppm, in $CDCl_3$): 16.02 (s, br), 0.59 (s, br, 15H, Cp*), −2.35 (s, br, 6H, ethyl CH_3), −13.48 (s, br, 15H, Cp*). Unit-resolution mass spectrum: parent envelope at *m/z* 581 (base peak), no fragmentation. Anal. Calcd for $CoFeBrC_{26}B_3H_{42}$: C, 53.68; H, 7.28. Found: C, 53.77; H, 7.66.

Synthesis of Cp*Fe($Et_2C_2B_3H_3$)CoCp (2). The same procedure was followed using 487 mg (2.0 mmol) of Cp*Co($Et_2C_2B_3H_3$) and equivalent quantities of $FeCl_2$ and Cp*Li. Chromatography on silica in hexane afforded a greasy brown band of decomposition products and a yellow fraction of starting material. Elution of the column with toluene gave brown solid **2**, 220 mg (0.51 mmol, 43% based on starting

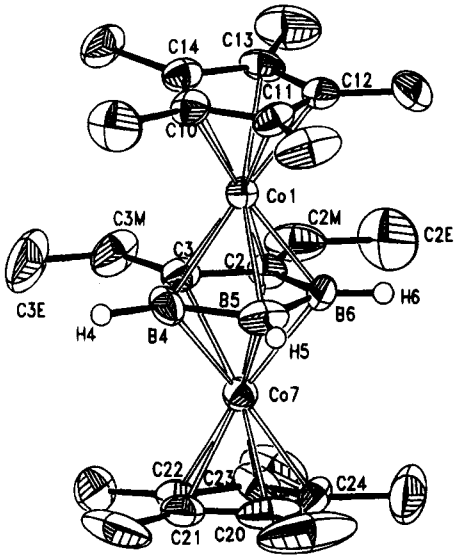

Figure 9. ORTEP drawing of the $3a^-$ anion with 50% thermal ellipsoids, with H atoms omitted except for those on boron (shown as spheres of arbitrary radius).

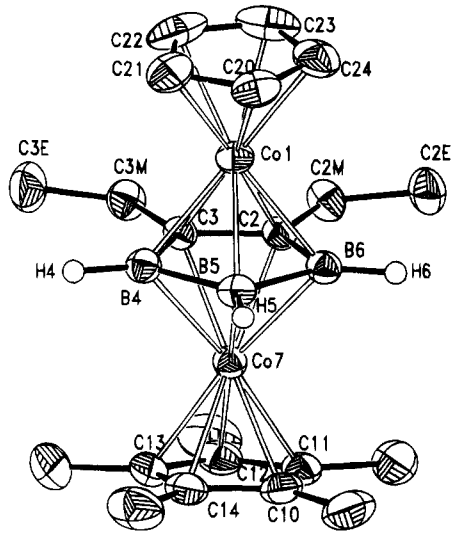

Figure 10. ORTEP drawing of **4**, presented as in Figure 9.

Table 3. Experimental X-ray Diffraction Parameters and Crystal Data

compound	$3a^-K(C_4H_8O)(C_{12}H_{24}O_6)^+$	**4**
empirical formula	$Co_2KO_7C_{42}B_3H_{75}$	$Co_2C_{21}B_3H_{33}$
fw	881.4	435.8
wavelength, Å	0.7107	0.7107
T, °C	20	20
space group	$P2_12_12_1$	$P2_1/c$
a, Å	15.252(14)	8.694(4)
b, Å	15.54(2)	21.049(11)
c, Å	20.25(2)	11.870(8)
β, deg		101.15(4)
V, Å^3	4801	2131
Z	4	4
μ, cm^{-1} (Mo Kα)	8.20	15.58
D(calcd), g cm^{-3}	1.219	1.358
final R indices[a] ($I > 2\sigma_I$)	R1 = 0.0463, wR2 = 0.0842	R1 = 0.0386, wR2 = 0.0898
R indices (all data)	R1 = 0.1048, wR2 = 0.1024	R1 = 0.0680, wR2 = 0.1025

[a] $R1 = \sum(||F_o| - |F_c||)/\sum|F_o|$ and $wR2 = \{[w(F_o^2 - F_c^2)^2]/\sum[w(F_o^2)^2]\}^{1/2}$.

cobaltacarborane consumed). Unit-resolution mass spectrum: parent envelope at m/z 433 (base peak). ^{1}H NMR (200 MHz) (δ, ppm, in THF-d_8): 5.60 (s, 5H, Cp), −0.60 (d, 3H, ethyl CH_3), −10.34 (s, 15H, Cp*). ESR (toluene, 4.3 K): $g_{\parallel} = 2.38$ and $g_{\perp} = 2.04$. Anal. Calcd for $CoFeC_{26}B_3H_{43}$: C, 58.29; H, 7.69. Found: C, 57.95; H, 8.03.

Table 4. Selected Bond Distances (Å) and Angles (deg) for $3a^-$

Co(1)−C(2)	2.111(9)	Co(7)−C(20)	2.036(6)
Co(1)−C(3)	2.078(9)	Co(7)−C(21)	2.067(11)
Co(1)−B(4)	2.040(11)	Co(7)−C(22)	2.149(10)
Co(1)−B(5)	2.138(8)	Co(7)−C(23)	2.083(10)
Co(1)−B(6)	2.090(11)	Co(7)−C(24)	2.056(10)
Co(1)−C(10)	2.057(9)	C(2)−C(3)	1.443(10)
Co(1)−C(11)	2.046(5)	C(3)−B(4)	1.569(14)
Co(1)−C(12)	2.067(9)	B(4)−B(5)	1.684(14)
Co(1)−C(13)	2.105(9)	B(5)−B(6)	1.65(2)
Co(1)−C(14)	2.103(10)	C(2)−B(6)	1.49(2)
Co(7)−C(2)	2.087(8)	C(2)−C(2M)	1.524(11)
Co(7)−C(3)	2.121(9)	C(2M)−C(2E)	1.508(13)
Co(7)−B(4)	2.133(11)	C(3)−C(3M)	1.533(11)
Co(7)−B(5)	2.147(8)	C(3M)−C(3E)	1.511(13)
Co(7)−B(6)	2.092(12)		
C(2)−C(3)−B(4)	112.5(9)	C(3)−C(2)−C(2M)	121.6(9)
C(3)−B(4)−B(5)	104.9(7)	C(2)−C(2M)−C(2E)	115.0(8)
B(4)−B(5)−B(6)	101.7(6)	Co(1)−C(3)−Co(7)	102.7(4)
B(5)−B(6)−C(2)	109.5(7)	Co(1)−C(3)−C(3M)	128.8(6)
B(6)−C(2)−C(3)	111.3(8)	Co(7)−C(3)−C(3M)	128.3(6)
B(6)−C(2)−C(2M)	126.9(8)	C(2)−C(3)−C(3M)	119.2(8)
Co(1)−C(2)−Co(7)	102.7(3)	B(4)−C(3)−C(3M)	128.3(8)
Co(1)−C(2)−C(2M)	127.2(6)	C(3)−C(3M)−C(3E)	114.1(9)
Co(7)−C(2)−C(2M)	130.0(6)		

Table 5. Selected Bond Distances (Å) and Angles (deg) for **4**

Co(1)−C(2)	2.073(3)	Co(7)−C(10)	2.020(3)
Co(1)−C(3)	2.071(3)	Co(7)−C(11)	2.062(3)
Co(1)−B(4)	2.090(4)	Co(7)−C(12)	2.089(3)
Co(1)−B(5)	2.081(4)	Co(7)−C(13)	2.059(3)
Co(1)−B(6)	2.094(4)	Co(7)−C(14)	2.020(3)
Co(1)−C(20)	2.010(3)	C(2)−C(3)	1.471(4)
Co(1)−C(21)	2.025(4)	C(3)−B(4)	1.554(5)
Co(1)−C(22)	2.062(4)	B(4)−B(5)	1.725(5)
Co(1)−C(23)	2.074(4)	B(5)−B(6)	1.710(5)
Co(1)−C(24)	2.040(4)	C(2)−B(6)	1.554(5)
Co(7)−C(2)	2.102(3)	C(2)−C(2M)	1.514(4)
Co(7)−C(3)	2.094(3)	C(2M)−C(2E)	1.518(5)
Co(7)−B(4)	2.086(4)	C(3)−C(3M)	1.518(4)
Co(7)−B(5)	2.066(4)	C(3M)−C(3E)	1.501(5)
Co(7)−B(6)	2.086(4)		
C(2)−C(3)−B(4)	113.3(3)	C(3)−C(2)−C(2M)	120.0(3)
C(3)−B(4)−B(5)	105.1(3)	C(2)−C(2M)−C(2E)	115.3(3)
B(4)−B(5)−B(6)	102.9(3)	Co(1)−C(3)−Co(7)	98.28(13)
B(5)−B(6)−C(2)	105.8(3)	Co(1)−C(3)−C(3M)	129.3(2)
B(6)−C(2)−C(3)	112.8(2)	Co(7)−C(3)−C(3M)	132.3(2)
B(6)−C(2)−C(2M)	127.2(3)	C(2)−C(3)−C(3M)	119.5(3)
Co(1)−C(2)−Co(7)	97.94(12)	B(4)−C(3)−C(3M)	127.2(3)
Co(1)−C(2)−C(2M)	129.1(2)	C(3)−C(3M)−C(3E)	115.3(3)
Co(7)−C(2)−C(2M)	132.9(2)		

Synthesis of Cp*Co($Et_2C_2B_3H_3$)CoCp* (3a). A 520 mg (1.64 mmol) sample of Cp*Co($Et_2C_2B_3H_5$) was deprotonated as described above at −10 °C in THF, warmed to room temperature, and treated with $(Cp^*CoBr)_2$. Workup of the product as in the previous syntheses gave 373 mg (0.73 mmol, 45% yield) of red crystalline **3a**. ^{1}H NMR (200 MHz, δ, ppm, in THF-d_8): 2.50 (q, 4H, ethyl CH_2, J_{HH} = 7.5 Hz), 1.56 (s, 15H, Cp*Co), −1.51 (t, 6H, ethyl CH_3, J_{HH} = 7.5 Hz). ^{13}C NMR (75.5 MHz, δ, ppm, in THF-d_8): 94.5 (br, cage carbons), 87.60 (Cp* ring carbons), 24.16 (ethyl CH_2), 16.11 (methyl CH_2), 10.14 (Cp* CH_3). ^{11}B NMR (115.8 MHz, proton-decoupled, δ, ppm, in THF-d_8): 48.0 (1B), 6.0 (2B). Anal. Calcd for $Co_2C_{26}B_3H_{43}$: C, 61.73; H, 8.57. Found: C, 61.76; H, 8.19.

Reduction of 3a to the Monoanion. A 1 mmol sample of **3a** in THF was exposed to a potassium mirror in an NMR tube in the presence of an excess of crown ether, producing a color change from brown-red to dark green. The solution was filtered in vacuo through a frit and concentrated via evaporation until saturation was reached. Storage for several days under refrigeration at 4 °C produced crystals suitable for X-ray diffraction analysis.

Chemical Oxidation of Neutral Complexes. The monocations were prepared via treatment of the neutral compound with 1 equiv of $AgBF_4$ in THF in a drybox. The solvent was removed in vacuo, the residue was dissolved in toluene, and the solution was filtered through a fine glass frit. The insoluble ionic product and silver metal remaining on the frit were washed with 20 mL of toluene, following which the metallacarborane BF_4^- salt was washed through the frit with CH_2Cl_2 or $CHCl_3$ and dried under vacuum. The air-stable salts were then employed in NMR correlation studies as described above. Purity of the salts was established by elemental analysis. Anal. Calcd for $\mathbf{3b}^+BF_4^-$, $Co_2F_4C_{24}B_4H_{39}$: C, 51.05; H, 6.96. Found: C, 50.48; H, 6.67.

X-ray Structure Determinations. Diffraction data were collected on a Siemens-Stoe AED2 diffractometer at room temperature using Mo Kα radiation. The structures were solved by direct methods (SHELXS86[22]) and refined by full-matrix least-squares based on F^2 (SHELXL93[22]) using anisotropic thermal parameters for non-hydrogen atoms. The hydrogen atoms on boron were located and refined isotropically. All other hydrogen atoms were included in calculated positions or treated as part of a rigid group (CH_3), and only common isotropic temperature factors were refined. Crystallographic data and details of the structure determination are given in Table 3.

(22) Sheldrick, G. M. SHELXS86 (1986) and SHELXL93 (1993). Universität Göttingen.

Acknowledgment. This work was supported by the National Science Foundation, Grant No. CHE 9022713 (to R.N.G.), the U.S. Army Research Office (to R.N.G.), and a grant to M.S. from the Deutsche Forschungsgemeinschaft. We thank Dr. Tom Sutto for recording the Mössbauer spectra.

Supplementary Material Available: Tables of atomic coordinates (including observed and calculated hydrogen atom positions), isotropic and anisotropic displacement parameters, bond distances and angles, and calculated mean planes for $\mathbf{3a}^-$ and **4**, an ORTEP drawing of the cation in the $\mathbf{3a}^-$ salt, a drawing of the molecular structure and tables of crystal data and structure refinement, atomic coordinates, bond lengths and angles, anisotropic displacement parameters, and hydrogen coordinates and isotropic displacement parameters for the neutral complex **3a**, and tables of ^1H and ^{13}C NMR data from paramagnetic NMR correlation experiments (34 pages). Ordering information is given on any current masthead page.

IC941239H